Supporting Online Material for

HD 181068: A Red Giant in a Triply Eclipsing Compact Hierarchical Triple System

A. Derekas,* L. L. Kiss, T. Borkovits, D. Huber, H. Lehmann, J. Southworth, T. R. Bedding, D. Balam, M. Hartmann, M. Hrudkova, M. J. Ireland, J. Kovács, Gy. Mezö, A. Moór, E. Niemczura, G. E. Sarty, Gy. M. Szabó, R. Szabó, J. H. Telting, A. Tkachenko, K. Uytterhoeven, J. M. Benkö, S. T. Bryson, V. Maestro, A. E. Simon, D. Stello, G. Schaefer, C. Aerts, T. A. ten Brummelaar, P. De Cat, H. A. McAlister, C. Maceroni, A. Mérand, M. Still, J. Sturmann, L. Sturmann, N. Turner, P. G. Tuthill, J. Christensen-Dalsgaard, R. L. Gilliland, H. Kjeldsen, E. V. Quintana, P. Tenenbaum, J. D. Twicken

*To whom correspondence should be addressed. E-mail: derekas@konkoly.hu

Published 8 April 2011, *Science* **332**, 216 (2011)
DOI: 10.1126/science.1201762

This PDF file includes:

Materials and Methods
Figs. S1 to S3
Tables S1 to S3
References

Other Supporting Online Material for this manuscript includes the following:
available at www.sciencemag.org/cgi/content/full/332/6026/216/DC1

SOM Data (available as a zipped file)

A. Derekas[1,2,3*], L.L. Kiss[2,4], T. Borkovits[5,6], D. Huber[4], H. Lehmann[7], J. Southworth[8], T.R. Bedding[4], D. Balam[9], M. Hartmann[6], M. Hrudkova[6], M.J. Ireland[4], J. Kovács[10], Gy. Mező[2], A. Moór[2], E. Niemczura[11], G.E. Sarty[12], Gy.M. Szabó[2], R. Szabó[2], J.H. Telting[13], A. Tkachenko[6], K. Uytterhoeven[14,15], J.M. Benkő[2], S.T. Bryson[16], V. Maestro[4], A. E. Simon[2], D. Stello[4], G. Schaefer[17], C. Aerts[18,19], T.A. ten Brummelaar[17], P. De Cat[20], H.A. McAlister[17], C. Maceroni[21], A. Mérand[22], M. Still[16], J. Sturmann[17], L. Sturmann[17], N. Turner[17], P.G. Tuthill[4], J. Christensen-Dalsgaard[23], R.L. Gilliland[24], H. Kjeldsen[23], E.V. Quintana [25], P. Tenenbaum[25], J.D. Twicken[25]

[1]Department of Astronomy, Eötvös University, Budapest, Hungary, E-mail: derekas@konkoly.hu

[2]Konkoly Observatory, Hungarian Acadamey of Sciences, H-1525 Budapest, PO Box 67, Hungary

[3]Magyary Zoltán Postdoctoral Research Fellow

[4]Sydney Institute for Astronomy (SIfA), School of Physics, University of Sydney, NSW 2006, Australia

[5]Baja Astronomical Observatory, H-6500 Baja, Szegedi út, Kt. 766, Hungary

[6]Eötvös József College, H-6500 Baja, Szegedi út 2, Hungary

[7]Thüringer Landessternwarte Tautenburg, Karl-Schwarzschild-Observatorium, 07778 Tautenburg, Germany

[8]Astrophysics Group, Keele University Newcastle-under-Lyme, ST5 5BG, UK

[9]Dominion Astrophysical Observatory, Herzberg Institute of Astrophysics,5071 West Saanich Road, Victoria, BC, V9E 2E7, Canada

[10]Gothard Observatory, Eötvös University, H-9704 Szombathely, Szent Imre Herceg u. 112., Hungary

[11]Astronomical Institute, Wrocław University, Kopernika 11, 51-622 Wrocław, Poland

[12]Department of Physics and Engineering Physics, University of Saskatchewan, 9 Campus Drive, Saskatoon, Saskatchewan S7N 5A5, Canada

[13]Nordic Optical Telescope, Apartado 474, 38700 Santa Cruz de La Palma, Spain

[14]Lab. AIM, CEA/DSM-CNRS-Université Paris Diderot; CEA, IRFU, SAp, Saclay, 91191, Gif-sur-Yvette, France

[15]Kiepenheuer-Institut für Sonnenphysik, Schneckstr. 6, 79104 Freiburg, Germany [16]NASA Ames Research Center, Moffett Field, CA 94035, USA

[17]Center for High Angular Resolution Astronomy, Georgia State University, PO Box 3969, Atlanta, Georgia 30302-3969, USA

[18]Instituut voor Sterrenkunde, Katholieke Universiteit Leuven, Celestijnenlaan 200 D, 3001 Leuven, Belgium

[19]IMAPP, Department of Astrophysics, Radboud University Nijmegen, P.O. Box 9010, NL-6500 GL Nijmegen, The Netherlands

[20]Royal Observatory of Belgium, Ringlaan 3, 1180 Brussel, Belgium

[21]INAF - Osservatorio astronomico di Roma, via Frascati 33, I-00040 Monteporzio C., Italy

[22]European Southern Observatory, Alonso de Córdova 3107, Casilla 19001, Santiago 19, Chile

[23]Department of Physics and Astronomy, Building 1520, Aarhus University, 8000 Aarhus C, Denmark

[24]Space Telescope Science Institute, 3700 San Martin Drive, Baltimore, MD 21218, USA

[25]SETI Institute, Moffett Field, CA 94035, USA

*To whom correspondence should be addressed; E-mail: derekas@konkoly.hu

Sections to the Supporting Online Material

1 Observations and methods

1.1 Lucky Imaging

We checked HD 181068 for resolved optical companions with lucky imaging on the 1m RCC telescope of the Konkoly Observatory. For this, we took over 100,000 short-exposure frames on 2010 June 28/29 and June 29/30, using an Andor IXon^{EM}+888 EMCCD, with exposure times of 30–61 ms in $UBV(RI)_{\rm C}$ filters. The median seeing was about 1.6″. In each filter we obtained 10,000–30,000 frames, from which the best 0.3% was selected and combined. The resulting images show clean single-star profiles with typical FWHM of 0.9″ in U, 0.64″ in V and 0.45″ in $I_{\rm C}$. For the latter, we have also determined contrast limits at representative separations. An analysis of simulated artificial stars with a wide range of brightnesses and separations resulted in the following upper limits to the magnitude difference of a hypothetic optical companion: 0.4″ – 2.1 mag; 0.8″ – 2.9 mag;1.2″ – 5 mag; 2.0″ – 6.4 mag.

1.2 Spectroscopy

To measure the orbital motion of HD 181068 A, we acquired optical spectra at four different observatories. We obtained 38 spectra in total, as follows: 6 spectra with the FIES spectrograph at the Nordic Optical Telescope (NOT; resolution 47 000, wavelength range 3623–7270 Å); 11 spectra at the Dominion Astrophysical Observatory (DAO; resolution 10 000 and wavelength range 4300–4556 Å); 16 spectra with the 2-m telescope at the Thüringer Landessternwarte (TLS) in Tautenburg (resolution 66 000, wavelength range 4700–7400 Å); and 5 spectra at the McDonald Observatory (McD) using the 2.7m telescope and the Robert G. Tull coudé spectrograph (resolution 60 000 and wavelength range 3700–10000 Å).

From the light curve, we know that HD 181068 A contributes almost all the light of the triple system. We fitted theoretical template spectra from the library of (*S1*) to a NOT spectrum

and determined the following parameters: $T_{\rm eff} = 5100 \pm 200$ K, $\log g = 2.8 \pm 0.3$, $[M/H] = -0.6 \pm 0.3$ and $v \sin i = 14$ km s^{-1}. These values are all in good agreement with those of (*S2*). As a check, we can also use Strömgren photometry from (*S3*): $V = 7.091$, $b - y = 0.586$, $m_1 = 0.296$ and $c_1 = 0.399$. From these quantities and the calibration of (*S4*), we find: $T_{\rm eff} = 5200$ K, $E(b-y) = 0.087$ and $(b-y)_0 = 0.499$. These numbers are consistent with the spectroscopic results and confirm that HD 181068 A is a G-type giant star.

We have used one high-quality NOT spectrum to measure the width of the Ca II K emission line at 3934 Å. This has been done interactively with the IRAF task SPLOT after converting the wavelength scale to Doppler velocities around the core of the emission. The measured value is $W_0 = 72.8$ km s^{-1}, which was then used to calculate the V-band absolute magnitude via the calibration of the Wilson-Bappu effect by (*S5*).

Radial velocities were determined using the IRAF task FXCOR. The template for all but the TLS spectra was selected from (*S1*), with closely matching parameters, which ensured that no systematic errors were introduced by spectral template mismatch. The 16 TLS RVs have been determined in a first step from cross-correlation with the mean spectrum that was iteratively built from the single spectra by shift-and-add according to the measured RVs. This mean spectrum was then analysed using the program LLMODELS (*S6*) to compute a grid of stellar atmosphere models and the program SYNTHV (*S7*) to compute the synthetic spectra. We found $T_{\rm eff} = 5300 \pm 100K$, $\log g = 2.8 \pm 0.2$ dex, $[M/H] = -0.2 \pm 0.1$, and $v \sin i = 14 \pm 1$ km s^{-1}. Finally, we used the best-fit synthetic spectrum as a template for cross-correlation to determine the RVs of the TLS spectra on an absolute scale. Depending on the instrument and the spectra, the velocities are accurate to $\pm$0.5–2 km s^{-1}. The observed radial velocities and their deviations from the orbital fit are listed in Table S1.

The orbital solution (see Fig. S1) was calculated by the method of differential corrections. We omitted the DAO RVs because they show a much larger scatter around the calculated orbital curve, despite being observed during the same epoch as the other instruments. The eccentricity

Table S1: The list of radial velocity measurements. The typical uncertainty is ± 1 km s^{-1}. Sources: 1=TLS, 2=NOT, 3=MCD, 4=DAO

BJD 2455000+	phase	RV (km s^{-1})	O$-$C	Source
358.53084	0.8900	31.19	0.52	1
369.55796	0.1323	-20.24	0.26	2
369.69747	0.1353	-20.79	0.18	2
404.79220	0.9063	27.72	0.11	3
405.66236	0.9255	23.61	-0.15	3
407.80097	0.9724	16.33	2.96	4
408.70024	0.9922	9.19	0.40	3
408.79660	0.9943	7.37	-0.92	4
408.95076	0.9977	5.02	-2.49	4
409.73019	0.0148	3.26	-0.26	3
409.79654	0.0163	3.55	0.38	4
409.93630	0.0194	0.59	-1.87	4
410.85279	0.0395	-2.27	-0.10	3
410.87936	0.0401	-2.46	-0.17	4
412.38515	0.0732	-9.66	-0.14	2
413.37500	0.0949	-14.06	-0.14	2
413.39495	0.0953	-14.14	-0.14	2
414.37817	0.1169	-17.97	-0.01	2
428.30911	0.4230	-10.01	0.32	1
428.61223	0.4297	-8.82	0.11	1
429.58763	0.4511	-4.58	-0.30	1
430.31478	0.4671	-0.25	0.42	1
430.61761	0.4737	0.52	-0.34	1
431.45537	0.4921	5.18	0.05	1
431.52041	0.4935	5.37	-0.09	1
434.78970	0.5654	22.54	0.73	4
434.92856	0.5684	25.72	3.25	4
435.80118	0.5876	27.40	0.98	4
436.77665	0.6090	30.98	0.48	4
437.78550	0.6312	33.88	-0.39	4
440.39439	0.6885	41.35	-0.06	1
455.28666	0.0157	3.32	0.01	1
457.44107	0.0630	-7.65	-0.28	1
458.39301	0.0839	-11.98	-0.24	1
460.25545	0.1248	-19.24	0.06	1
461.25709	0.1468	-22.56	0.11	1
462.27140	0.1691	-25.52	0.00	1
463.34313	0.1927	-28.09	-0.26	1

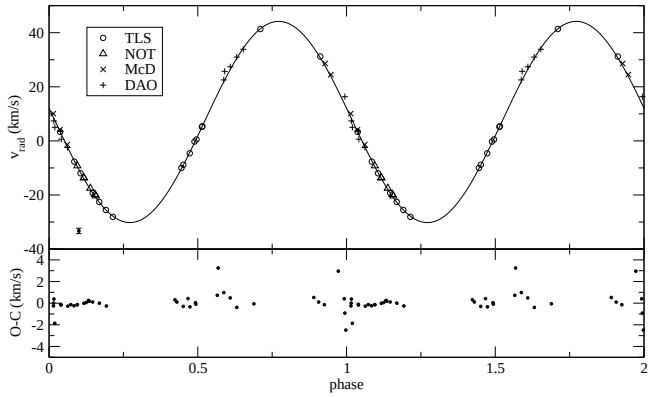

Figure S1: Measured RVs versus the orbital phase (45.5 d) for the TLS (circles), NOT (triangles), McDonald (McD, crosses), and DAO (pluses) observations. The vertical bar in the lower left corner shows the size of the representative ± 1 km s^{-1} uncertainty.

from the fit was $e = 0.022 \pm 0.023$, which is consistent with zero, and in the final solution we set $e = 0$ because its inclusion as a free parameter did not improve the solution. We also fixed the orbital period to that obtained from the light-curve fitting (a free search gives a slightly different value but does not improve the quality of the solution). Table 1 lists the derived orbital elements. In the corresponding solution, we corrected the NOT RVs by -0.35 km s^{-1} and the McDonald RVs by -0.70 km s^{-1} with respect to the TLS RVs. This correction minimized the rms to 214 m s^{-1}, and its influence on the derived elements was only marginal.

1.3 Interferometry

Interferometric observations were performed on three nights in 2010 July, using two different baselines (156.3 m and 248.1 m) of the CHARA Array. All the observations were performed outside the long-period eclipses, meaning that some flux from the BC pair was present during all observations. With an eclipse depth of only 1%, however, the companions are much fainter than the primary and are negligible in our analysis. The raw data were reduced using the PAVO data analysis pipeline.

We obtained 7 scans of HD181068 over 23 wavelength channels spanning from 0.65 to 0.8

mum each, yielding a total of 161 V2 measurements. We observed six stars of spectral type A0 to calibrate the raw visibilities. All stars were located within 5° in the sky and their estimated diameters were at least a factor of 2 smaller than HD 181068A. Inspection of the data revealed that three of the calibrators (HD179395, HD182487 and HD181521) are potential binaries and could not be used for calibration. The remaining three stars used to calibrate our data were HD179733, HD180138 and HD184787. To determine the angular diameter of HD181068 A a limb-darkened disc model (*S8*) was fitted to the calibrated visibilities. The corresponding linear limb-darkening coefficient was determined by interpolating the spectroscopically determined values of $\log\ g$ and $T_{\rm eff}$ in the grid of (*S9*), yielding $\mu = 0.63 \pm 0.02$. The resulted angular diameter of HD181068 A is $\theta_{LD} = 0.461 \pm 0.011$ milli-arcsecond.

The uncertainty on the diameter was estimated using 40000 Monte-Carlo simulations as follows: For each simulation, we drew realizations corresponding to Gaussian distributions for the calibrator angular diameters, limb-darkening coefficient and wavelength channels, with assumed standard deviations of 5%, 3% and 0.5%. With these parameters we then calibrated the raw visibility measurements and fitted an angular diameter to the calibrated data using least-squares minimization. To account for random errors, including correlations between wavelength channels, we perturbed this fit by adding random numbers generated from the empirical covariance matrix of the data and then repeated the fit (*S10*). The final uncertainty was taken as the standard deviation of the resulting total distribution, scaled by square root of the reduced χ^2 value (2.5) as determined from the fit to the original data. The measurements of the 7 scans averaged over 23 wavelength channels are listed in Table S2.

1.4 HD 181068 B and C

We have constrained the parameters of the BC pair by modelling the short-period eclipses in the Kepler band. First, we removed the long-term variations of the uneclipsed brightness in the light curve by fitting spline function polynomials and removing data obtained during the long-period

Table S2: Calibrated interferometric measurements of HD181068 averaged over 23 wavelength channels for each scan. The full list of measurements are available from the authors on request.

JD-2451545	Projected Baseline (m)	Spatial Frequency ($\times 10^8 rad^{-1}$)	avg(V^2)	avg(σV^2)
3837.973	144.064	2.010901	0.648	0.040
3838.000	140.892	1.966629	0.593	0.043
3852.920	247.766	3.458418	0.270	0.050
3852.930	247.654	3.456854	0.252	0.053
3853.929	247.640	3.456666	0.252	0.044
3853.944	247.378	3.452999	0.210	0.057
3853.969	246.584	3.441913	0.204	0.054

eclipses. In this way, the light from star A was assigned to be the 'third light' component. The parameters of the BC pair were deduced by modelling the short-period eclipses in the Kepler band using the JKTEBOP code (*S11, S12*). A preliminary fit was performed, allowing a few outlying data points to be identified and removed. A detailed fit was then made, using numerical integration to account for the 30-minute long duration of individual observations. Uncertainties in the parameters of the fit were calculated using 1000 Monte Carlo simulations (*S13*). In each simulation, a synthetic dataset was created by evaluating the best-fitting model at the observed times and adding Gaussian noise. This was then fitted in the same way as the real data, starting from initial parameter values which were perturbed versions of the best-fitting parameter values. The error estimate for each fitted parameter was then evaluated by taking the inner 68.3% of all the values of the parameter found from the synthetic datasets. The resulting photometric parameters are given in Table S3.

We found the ratio of the radii of the B and C components to be poorly constrained at present, partly due to the low sampling rate of the *Kepler* long-cadence data. The A component contributes 99.29% of the system light in the *Kepler* passband, and the BC pair contribute 0.44% and 0.27%, respectively. Taking the V-band absolute magnitude of HD 181068 A to be $M_V(\mathrm{A}) = -0.3$ and assuming that our results for the *Kepler* passband are representative of the V-band, we find $M_V(\mathrm{B}) = 5.6$ and $M_V(\mathrm{C}) = 6.1$. Such absolute magnitudes indicate spectral

Table S3: Photometric parameters obtained for the short-period eclipses, using standard symbols in the study of eclipsing binary systems. $L_{\rm A}$, $L_{\rm B}$ and $L_{\rm C}$ are all expressed as fractions of the total light of the system in the Kepler passband.

Parameter	Best fit	Uncertainty
$P_{\rm BC}$ (d)	0.9056770	0.0000026
$T_{\rm MinI}$ (BJD)	2455051.23625	0.00020
i_1 (degrees)	87.7	1.6
$(R_{\rm B}+R_{\rm C})/a_{\rm BC}$	0.3288	0.0044
$R_{\rm C}/R_{\rm B}$	1.01	0.13
$R_{\rm B}/a_{\rm BC}$	0.164	0.011
$R_{\rm C}/a_{\rm BC}$	0.165	0.011
$L_{\rm A}$	0.9929	0.0006
$L_{\rm B}$	0.0044	0.0007
$L_{\rm C}$	0.0027	0.0004

types of G8 V and K1 V for stars B and C, respectively.

We can only estimate masses of the BC pair based on the spectral type because there is no independent $T_{\rm eff}$ measurement of them. Fig. S2 shows a Hertzsprung-Russel Diagram with BASTI evolutionary tracks (*S14*) of different masses for $[M/H] = -0.25$ (as suggested from the spectroscopy), as well as the most likely locations of the components of the triple system. The position of the BC components was derived based on the spectral types stated above, assuming an error of 200 K in $T_{\rm eff}$ and 0.2 mag in absolute magnitude, respectively.

2 The variability of HD 181068 A

The light curve (see Fig. 1) shows slow variations with the same timescale as the long-period eclipses, which presumably arise from ellipsoidal distortion of the primary. We also see faster oscillations with the same timescale as the orbital period of the BC pair. These are visible both outside and during the eclipses and are less obvious to interpret.

To investigate this further, Fig. S3*a* shows the amplitude spectrum of the light curve after first removing observations made during both the long- and short-period eclipses. This procedure left a light curve with a duty cycle slightly above 60%, and it introduced alias peaks in the

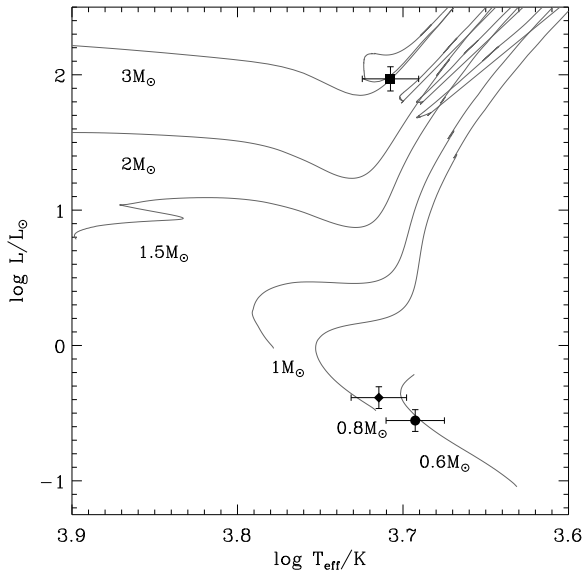

Figure S2: A Hertzsprung-Russell Diagram using the BASTI tracks (*S14*) for $[M/H] = -0.25$. It shows the locations of components A, B and C, marked by the filled square, diamond and circle, respectively.

amplitude spectrum at the multiples of the orbital frequencies. The strongest peak in the spectrum occurs at $25\ \mu$Hz, corresponding to half the orbital period of the BC binary. As mentioned, this periodicity is clearly visible in the light curve.

To search for other frequencies we used iterative sine-wave fitting (prewhitening) with Period04 (*S15*). In five steps, we measured and identified the following frequencies:

- $f_1 = 24.54\,\mu\mathrm{Hz} = 2(f_{\mathrm{short}} - 2f_{\mathrm{long}})$
- $f_2 = 25.05\,\mu\mathrm{Hz} = 2(f_{\mathrm{short}} - f_{\mathrm{long}})$
- $f_3 = 25.56\,\mu\mathrm{Hz} = 2f_{\mathrm{short}}$
- $f_4 = 51.12\,\mu\mathrm{Hz} = 4f_{\mathrm{short}}$
- $f_5 = 12.83\,\mu\mathrm{Hz} = f_{\mathrm{short}} + 1/T_{\mathrm{obs}}$

Here, $f_{\mathrm{short}} = 1/P_{\mathrm{BC}}$, $f_{\mathrm{long}} = 1/P_{\text{A-BC}}$, and T_{obs} is the time span of observations. Fig. S3*b* shows the amplitude spectrum after the slow variations and these five strongest peaks have been

subtracted from the time series.

Could the observed signal in HD 181068 arise from solar-like oscillations? According to the parameters derived from the interferometry and spectroscopy, HD 181068 A is a red giant star located in the bottom of the red giant branch. Studies of similar red giants with *Kepler* (*S16,S17*) show that essentially all stars in this region of the H-R diagram exhibit solar-like oscillations that appear as a broad power excess centred at a characteristic frequency $\nu_{\rm max}$ and composed of a regularly spaced series of peaks. Using the scaling relation of (*S18*) with the derived values of mass, radius and effective temperature, we estimate $\nu_{\rm max} = 64 \pm 16$ μHz for HD 181068 A, while the expected amplitude is about 80 ppm.

For comparison, Fig. S3*c* shows the amplitude spectrum of a typical red giant with $\nu_{\rm max} \sim 80$ μHz (KIC 12507577). To make the comparison exact, we calculated this amplitude spectrum using exactly the same portions of the light curve that were used for HD 181068 in Fig. S3*a*. In KIC 12507577 we see the regular peaks that characterize solar-like oscillations, whereas in HD 181068 A we see just a few peaks whose removal (Fig. S3*b*) leaves only a slowly rising power distribution. The observed signal in HD 181068 A is clearly not compatible with solar-like oscillations. Indeed, the solar-like oscillations that we would expect to see in a giant of this type seem to have been suppressed.

The frequency content of the light curve suggests an intimate link to the orbital frequencies in the triple system. We are led to suggest that we are seeing tidally-induced oscillations that are driven by the orbital motion of the BC pair. Tidally-induced oscillations have previously been reported in a few binary systems (*S19, S20, S21*), but here the situation is different because the period of the oscillations does not correspond to the orbit of the A component, but rather to that of the BC pair. While a fuller discussion of this possibility is postponed to a future publication, we note that the amplitude of tidally driven oscillations can be simply estimated by assuming that the brightness changes are proportional to the tidal heights given by $R_A\,((M_B + M_C)/M_A)\,(R_A/a)^3$, where a is the semimajor axis of the outer binary. Every num-

ber put together yield an estimated amplitude of 3 ppt, which is a factor of 10 larger than what we observe and a factor of 40 larger than the amplitude of solar-like oscillations.

3 Supplemented data files

In addition to this document describing the supporting extra material, we also make all the data mentioned throughout the paper and SOM available to the general community at the webpage of the journal. The full list of datafiles that are stored in a single compressed tarball file is the following:

```
1201762som_sed.txt           Spectral Energy Distribution (Main text)
1201762som_lucky_image.fits  I-band lucky image (SOM, 1.1)
1201762som_fies(1..6).fits   6 NOT/FIES spectra (SOM, 1.2)
1201762som_dao(1..11).fits   11 DAO spectra (SOM, 1.2)
1201762som_tls(1..16).fits   16 TLS spectra (SOM, 1.2)
                             (barycentric corrections applied)
1201762som_mcd(1..5).fits    5 McDonald spectra (SOM, 1.2)
```

References

S1. U. Munari, *et al.*, *Astron. Astrophys.* **442**, 1127 (2005)

S2. P. Guillout, *et al.*, *Astron. Astrophys.* **504**, 829 (2009)

S3. E.H. Olsen, *Astron. Astrophys. Suppl.* **102**, 89 (1993)

S4. T.T. Moon, M.M. Dworetsky, *Mon. Not. Royal Astron. Soc.* **217**, 305 (1985)

S5. G. Pace, *et al.*, *Astron. Astrophys.* **401**, 997 (2003)

S6. D. Shulyak, *et al.*, *Astron. Astrophys.* **428**, 993 (2004)

S7. V. Tsymbal, *ASP Conf. Series* **108**, 198 (1996)

S8. R. Hanbury Brown, *et al.*, *Mon. Not. Royal Astron. Soc.* **167**, 475 (1974)

S9. A. Claret, *Astron. Astrophys.* **363**, 1081 (2000)

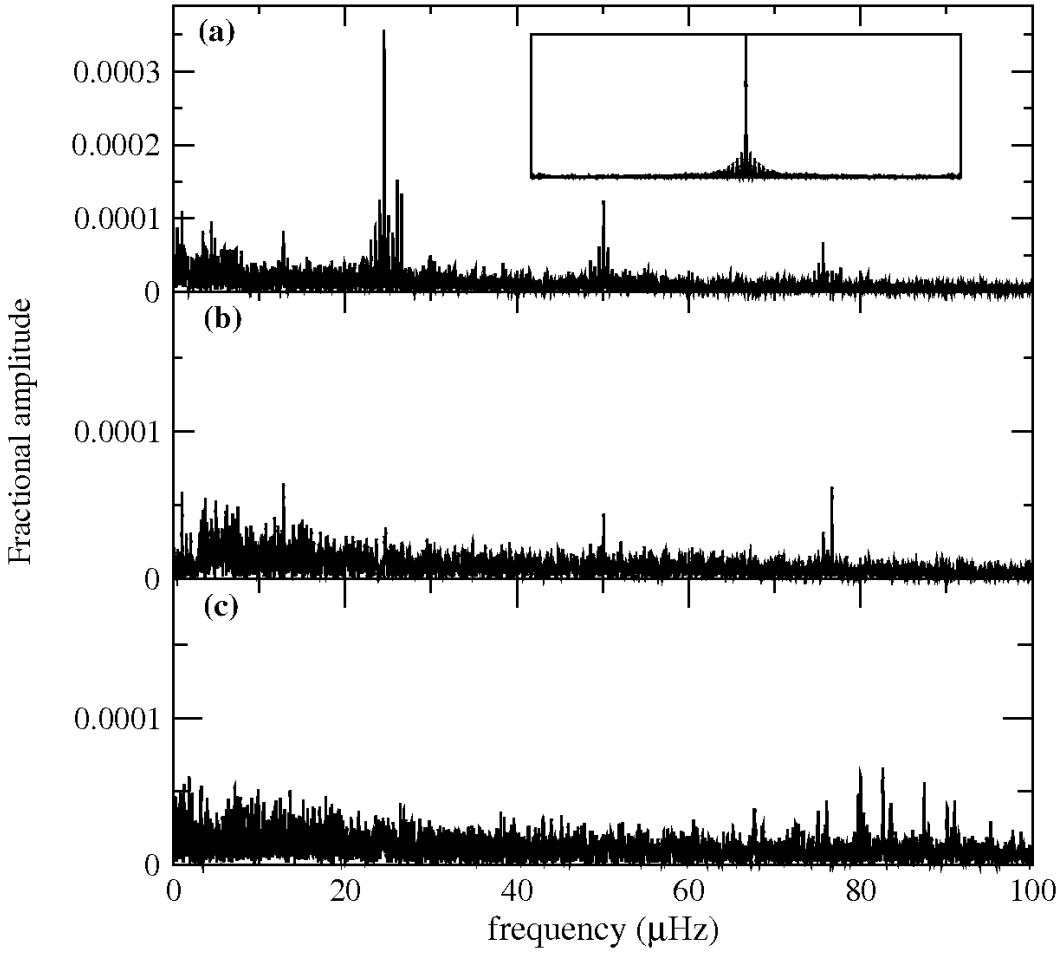

Figure S3: The amplitude spectrum of HD 181068 A and the change after five prewhitening steps (panels a and b). The inset shows the spectral window function with the same axis scales. Panel c: the spectrum of a typical red giant star (KIC 12507577), for which $\nu_{\rm max} \sim 80$ μHz. The vertical scale in panels b and c is increased by a factor of two.

S10. W.H. Press et al., Numerical Recipes in C, *Cambridge University Press* (1992)

S11. J. Southworth, *et al.*, *Mon. Not. Royal Astron. Soc.* **355**, 986 (2004)

S12. J. Southworth, *et al.*, *Mon. Not. Royal Astron. Soc.* **363**, 529 (2005)

S13. J. Southworth, *et al.*, *Mon. Not. Royal Astron. Soc.* **363**, 529 (2005)

S14. A. Pietrinferni, *et al.*, *Astrophys. Journal* **612**, 168 (2004)

S15. P. Lenz, M. Breger, *Comm. Asteroseis.* **146**, 53 (2005)

S16. D. Huber *et al.*, *Astrophys. Journal*, 723, 1607 (2010)

S17. T. Kallinger *et al.*, *Astron. Astrophys.*, 522, A1 (2010)

S18. H. Kjeldsen, T.R. Bedding, *Astron. Astrophys.* **293**, 87 (1995)

S19. P. De Cat, *et al.*, *Astron. Astrophys.* **355**, 1015 (2000)

S20. G. Handler, *et al.*, *Mon. Not. Royal Astron. Soc.* **333**, 262 (2002)

S21. C. Maceroni, *et al.*, *Astron. Astrophys.* **508**, 1375 (2009)